

Original article

CC BY 4.0

<https://doi.org/10.15828/2075-8545-2025-17-3-307-324>

# Nanostructured titanium dioxide-based photocatalysts for self-cleaning concrete: assessment of effects of phase composition on photocatalytic activity of TiO<sub>2</sub>

Artemy S. Balykov\* , Denis B. Chugunov , Vladimir M. Kyashkin , Natalia S. Davydova 

National Research Mordovia State University, Saransk, Russia

\* Corresponding author: e-mail: artbalrun@yandex.ru

## ABSTRACT

**Introduction.** Currently, the development of photocatalytically active cement-based materials with self-cleaning properties is a promising area of building materials science. Self-cleaning concrete is obtained by using photocatalytic additives, of which titanium dioxide (TiO<sub>2</sub>) is the most common. It has been found that the functional properties of TiO<sub>2</sub> depend largely on its phase composition. This study aimed to establish the patterns of influence of phase composition on the photocatalytic activity of titanium dioxide under the impact of artificial ultraviolet and natural solar radiation and to identify the most effective titanium oxide-based photocatalysts for subsequent use in the composition of self-cleaning concrete. **Methods and materials.** Four titanium dioxide samples, namely two industrial samples and two samples synthesized by hydrolysis of titanium alkoxide in acidified water-alcoholic medium followed by calcination at 500 °C, were the objects of the study. X-ray powder diffractometry was the method used to investigate the structure parameters of TiO<sub>2</sub> samples. The model reaction of oxidative degradation of methylene blue under UV- and daylight exposure was the means for studying the photocatalytic activity of titanium dioxide samples. **Results and discussion.** It was found that polymorphic modifications of titanium dioxide had a multidirectional effect on its functional characteristics, in particular, a rise in the content of anatase and rutile led to an increase and decrease in the photoactivity of TiO<sub>2</sub> samples, respectively. The single-phase sample with anatase structure was most effective under UV irradiation, while the three-phase sample with the anatase : brookite : rutile ratio of 67% : 13% : 20% had the highest activity under daylight exposure. The photocatalyst composition, including several polymorphs of TiO<sub>2</sub> with a predominance of anatase form (more than 50%), allowed to achieve a synergistic effect of increasing the photocatalytic activity of titanium dioxide under conditions of solar radiation due to the formation of type-II semiconductor heterojunctions. Heterostructures made it possible to improve the spatial separation of charge carriers and to reduce the recombination rate of photogenerated electron-hole pairs. **Conclusion.** The obtained results indicated the possibility of improving the functional characteristics of titanium oxide-based additives for self-cleaning concrete due to the targeted regulation of their phase composition by optimizing the synthesis parameters of photocatalytic modifiers.

**KEYWORDS:** self-cleaning concrete, photocatalyst, titanium dioxide, sol-gel method, photocatalytic activity, phase composition, crystallite size, nanostructures, heterojunction, polymorphism, anatase, brookite, rutile, X-ray diffraction

**ACKNOWLEDGMENTS:** The research was supported by grant from the Russian Science Foundation (project No. 23-79-01029), <https://rscf.ru/en/project/23-79-01029/>.

## FOR CITATION:

Balykov A.S., Chugunov D.B., Kyashkin V.M., Davydova N.S. Nanostructured titanium dioxide-based photocatalysts for self-cleaning concrete: assessment of effects of phase composition on photocatalytic activity of TiO<sub>2</sub>. *Nanotechnologies in Construction*. 2025;17(3):307–324. <https://doi.org/10.15828/2075-8545-2025-17-3-307-324>. – EDN: YVRFDW.

# Наноструктурированные фотокатализаторы на основе диоксида титана для самоочищающихся бетонов. Оценка влияния фазового состава на фотокаталитическую активность $TiO_2$

Артемий Сергеевич Балыков\* , Денис Борисович Чугунов , Владимир Михайлович Кяшкин ,  
Наталья Сергеевна Давыдова 

Национальный исследовательский Мордовский государственный университет им. Н.П. Огарева, Саранск, Россия

\* Автор, ответственный за переписку: e-mail: artbalrun@yandex.ru

## АННОТАЦИЯ

**Введение.** В настоящее время перспективным направлением строительного материаловедения является разработка фотокаталитически активных цементных материалов, обладающих способностью к самоочищению. Получение самоочищающихся бетонов достигается за счет использования фотокаталитических добавок, среди которых наибольшее распространение получил диоксид титана. Известно, что функциональные свойства  $TiO_2$  в значительной степени зависят от его фазового состава. Цель данного исследования – установить закономерности влияния фазового состава на фотокаталитическую активность диоксида титана в условиях воздействия искусственного ультрафиолетового и естественного солнечного излучений с выявлением наиболее эффективных титаноксидных фотокатализаторов для последующего применения в рецептуре самоочищающихся бетонов. **Методы и материалы.** Объектами исследования являлись четыре образца диоксида титана: два промышленных и два синтезированных путем гидролиза алкоксида титана в подкисленной водно-спиртовой среде с последующим прокаливанием при температуре 500 °С. Исследование параметров структуры образцов  $TiO_2$  выполнялось методом рентгеновской порошковой дифрактометрии. Фотокаталитическая активность образцов диоксида титана была изучена в модельной реакции окислительной деструкции метиленового синего при воздействии УФ- и дневного света. **Результаты и обсуждение.** Установлено, что полиморфные модификации диоксида титана оказывают разнонаправленное влияние на его функциональные характеристики: увеличение содержания анатаза и рутила приводит соответственно к повышению и снижению фотоактивности образцов  $TiO_2$ . При УФ-облучении наибольшую эффективность показал однофазный образец с анатазной структурой, а в условиях воздействия дневного света – трехфазный образец с соотношением анатаз : брукит : рутил = 67% : 13% : 20%. Наличие в составе фотокатализатора нескольких полиморфов  $TiO_2$  с преобладанием анатазной формы (более 50%) позволяет достичь синергетического эффекта повышения фотокаталитической активности диоксида титана в условиях воздействия солнечного излучения благодаря формированию полупроводниковых гетероструктур (гетеропереходов) II типа, способствующих улучшению сепарации и снижению скорости рекомбинации фотогенерированных электронно-дырочных пар. **Заключение.** Полученные результаты свидетельствуют о возможности улучшения функциональных характеристик титаноксидных добавок для самоочищающихся бетонов за счет направленного регулирования их фазового состава, что может быть достигнуто посредством оптимизации параметров синтеза фотокаталитических модификаторов.

**КЛЮЧЕВЫЕ СЛОВА:** самоочищающийся бетон, фотокатализатор, диоксид титана, золь-гель метод, фотокаталитическая активность, фазовый состав, размер кристаллитов, наноструктуры, гетеропереход, полиморфизм, анатаз, брукит, рутил, рентгеновская дифракция

**БЛАГОДАРНОСТИ:** исследование выполнено за счет гранта Российского научного фонда (проект № 23-79-01029), <https://rscf.ru/project/23-79-01029/>.

## ДЛЯ ЦИТИРОВАНИЯ:

Балыков А.С., Чугунов Д.Б., Кяшкин В.М., Давыдова Н.С. Наноструктурированные фотокатализаторы на основе диоксида титана для самоочищающихся бетонов. Оценка влияния фазового состава на фотокаталитическую активность  $TiO_2$ . *Нанотехнологии в строительстве*. 2025;17(3):307–324. <https://doi.org/10.15828/2075-8545-2025-17-3-307-324>. – EDN: YVRFDW.

## INTRODUCTION

The development of cement-based materials with high performance characteristics is a priority area of building materials science [1, 2]. The range of modern modified concretes is quite diverse and includes different types, in

particular, high-strength concrete [3, 4], self-compacting concrete [5, 6], fiber reinforced concrete [7–9], reactive powder concrete [10, 11], self-prestressing concrete [5, 12, 13], etc.

It is known that individual or complex application of chemical and mineral additives with different com-

position, dispersity, and mechanism of action allows to create high performance concrete. Effective types of additives are superplasticizers [14], superabsorbent polymers [15], microsilia [16], opal-cristobalite rocks [17], fly ash [18], expanding sulfoaluminate modifiers [5], carbonate rocks and calcined polymineral clays [19, 20], carbon-based modifiers [2, 21], etc. A special group of modifiers includes nanoscale photocatalytic additives that allow to obtain photocatalytically active cement-based materials [22–24] having the ability to self-clean and decompose atmospheric pollutants, antibacterial effect, etc. [25–27].

Nanostructured titanium dioxide, characterized by non-toxicity, chemical stability, and high activity under ultraviolet radiation exposure, is one of the effective types of photocatalysts [28–31]. Nevertheless, the high recombination rate of photogenerated charge carriers, as well as the narrowed spectral range of action with the band gap of known titanium dioxide polymorphs equal to 3.0–3.5 eV, are the main disadvantages of  $\text{TiO}_2$ . The wide band gap of titanium(IV) oxide requires solving the problem of its sensitization to visible light [32–34].

The photocatalytic properties of titanium(IV) oxide depend significantly on its phase composition. Currently, the compound polymorphism, which consists in the existence in nature of four main crystalline modifications of  $\text{TiO}_2$ , such as anatase, brookite, rutile, and  $\text{TiO}_2(\text{B})$ , is actively used to improve the functional characteristics of titanium oxide-based photocatalysts [35].

Anatase and rutile are the most studied polymorphs of titanium dioxide, these tetragonal phases are widely used in the obtaining of commercial photocatalysts. Brookite, characterized by an orthorhombic crystal lattice, is the least stable phase in the  $\text{TiO}_2$  isomorphous series, is relatively rare in nature and remains poorly understood. Nevertheless, the results of individual studies show that the photoactivity of brookite may exceed the characteristics of anatase and rutile due to the presence of traps preferred for photocatalytic reactions [36, 37]. The  $\text{TiO}_2(\text{B})$  phase, which is a mixture of monoclinic syngony crystals, was first synthesized in 1980 by hydrolysis of  $\text{K}_2\text{Ti}_4\text{O}_9$  followed by thermal treatment at 500 °C [38].  $\text{TiO}_2(\text{B})$  is the least dense polymorph of titanium dioxide. In addition,  $\text{TiO}_2(\text{B})$  is a less stable phase compared to anatase and rutile [35].

It is known that the presence of two or three polymorphic modifications in the titanium dioxide composition, in particular, anatase/brookite [39–41], anatase/rutile [42–44], brookite/rutile [45, 46], anatase/ $\text{TiO}_2(\text{B})$  [47, 48], and rutile/ $\text{TiO}_2(\text{B})$  [49], anatase/brookite/rutile [50–52], and anatase/rutile/ $\text{TiO}_2(\text{B})$  [53], makes it possible to form heterostructures with intercrystalline boundaries in multiphase composites. These heterojunctions contribute to an increase in the photocatalytic activity of  $\text{TiO}_2$  by improving the separation of charge carriers and reducing

the recombination rate of photoinduced electron-hole pairs [35, 37, 39, 40]. In particular, the works [37, 40] show that the combination of anatase and brookite in the nanocrystalline composite structure allows to increase the catalytic activity of the material in both oxidation and reduction reactions. The high functional efficiency of titanium dioxide polymorphism also manifests itself in the well-known commercial Degussa P25 photocatalyst, which is a mixture of anatase and rutile in the ratio of 3 : 1 or 4 : 1 [42, 44].

This study aimed to establish the patterns of influence of phase composition on the photocatalytic activity of titanium dioxide under the impact of artificial ultraviolet and natural solar radiation and to identify the most effective titanium oxide-based photocatalysts for subsequent use in the composition of self-cleaning concrete.

We completed the following tasks in order to achieve the goal of this study:

1. The effects of synthesis conditions on the structure parameters of  $\text{TiO}_2$  precursors obtained by hydrolysis of titanium alkoxide in acidified water-alcoholic medium were studied.
2. The kinetics of photodecomposition process of methylene blue in solution was investigated under conditions of exposure to ultraviolet radiation and solar radiation in the absence and presence of titanium oxide-based photocatalysts.
3. The effects of phase composition on the photocatalytic activity of titanium dioxide samples were researched under conditions of exposure to ultraviolet light and daylight.
4. The interrelations and regularities were established between the synthesis conditions, phase composition and photoactivity of  $\text{TiO}_2$ , which made it possible to optimize the prescription and technological parameters for obtaining effective titanium oxide-based photocatalysts for self-cleaning concrete.

## METHODS AND MATERIALS

### Synthesis of $\text{TiO}_2$ samples from hydrolyzed precursors

Titanium(IV) oxide samples were synthesized by sol-gel method, which involves hydrolysis of titanium alkoxide in acidified water-alcoholic medium followed by thermal treatment of the resulting precursor in the form of hydrated titanium oxide ( $\text{TiO}_2 \cdot n\text{H}_2\text{O}$ ).

At the initial stage of the synthesis, titanium tetraisopropoxide (TTIP, pure grade) was dissolved in anhydrous isopropyl alcohol ( $\text{C}_3\text{H}_7\text{OH}$ , pure grade), then 0.1 M  $\text{HNO}_3$  solution was added to the mixture in doses, after which the mixture was vigorously stirred for 2 hours. The ratio of the reaction mixture components by volume was  $V_{\text{TIP}} : V_{\text{C}_3\text{H}_7\text{OH}} : V_{\text{HNO}_3}^{0.1 \text{ M}} = 0.75 : 1.0 : 1.0$ . The sol-gel

synthesis product formed by hydrolysis aged at a given temperature for 5 hours. The final stages involved sequential filtration, washing, and drying of the precipitate to obtain TiO<sub>2</sub> precursor powder.

During the experimental study, the variable parameters of synthesis were temperature at mixing of solutions ( $T_{mixing}$ ) and temperature of gel aging ( $T_{aging}$ ). The variation levels of these parameters were 20 °C and 80 °C. The drying temperature ( $T_{drying}$ ) and drying time ( $t_{drying}$ ) of samples were constant at 80 °C and 2 hours, respectively.

Table 1 shows the synthesis parameters and labeling of TiO<sub>2</sub> precursor samples.

The P-TiO<sub>2</sub>-1 and P-TiO<sub>2</sub>-2 precursors were calcined at 500 °C for 4 hours to obtain titanium dioxide powders. The calcined samples were labeled according to the type of precursor used, namely TiO<sub>2</sub>-1 and TiO<sub>2</sub>-2. Two commercial (industrial) samples of titanium(IV) oxide, characterized by different phase composition and designated as TiO<sub>2</sub>-3 and TiO<sub>2</sub>-4, were control samples.

Table 2 shows the list of TiO<sub>2</sub> samples, which were the object of experimental study, as well as information on the technology for their obtaining.

### X-ray diffraction phase analysis of TiO<sub>2</sub> samples and their precursors

The phase composition of TiO<sub>2</sub> samples and their precursors was determined by X-ray powder diffractometry on the PANalytical Empyrean diffractometer (the

Netherlands). The shooting conditions included the use of CuK<sub>α</sub> radiation with wavelength  $\lambda = 1.5406 \text{ \AA}$ ,  $\theta$ – $2\theta$  scanning mode, shooting range  $2\theta = 5\text{--}75^\circ$ , angle step of  $0.0131^\circ$ , and exposure time at point of 200 seconds. The phases were identified using the Crystallography Open Database (COD).

The sizes of coherent scattering regions (CSR) of the main phases such as anatase, rutile, and brookite, were calculated from the X-ray diffraction analysis results to assess the crystallinity degree of TiO<sub>2</sub> samples. The average sizes of CSR (crystallites) of these phases were determined by the main diffraction peaks free from superposition, in particular, at  $2\theta = 25.3^\circ$  and  $2\theta = 37.9^\circ$  for anatase (in the absence and presence of brookite, respectively), at  $2\theta = 30.8^\circ$  for brookite, and at  $2\theta = 27.4^\circ$  for rutile. The classical Scherrer formula was used to calculate the crystallite size:

$$D = L_{cr} = \frac{K \cdot \lambda}{\beta \cdot \cos \frac{2\theta}{2}} \quad (1)$$

where  $D$  ( $L_{cr}$ ) is the average size of crystallites (CSR) of the analyzed phase,  $\text{\AA}$ ;

$K$  is the particle shape coefficient (Scherrer constant),  $K \approx 0.9\text{--}1.0$ ;

$\lambda$  is the wavelength of X-ray radiation,  $\lambda = 1.5406 \text{ \AA}$ ;

$\beta$  is the full width at half maximum (FWHM) for the analyzed diffraction peak of phase, radians;

$\theta$  is the X-ray diffraction angle, radians.

**Table 1.** Synthesis parameters and labeling of TiO<sub>2</sub> precursor samples

Sample number	Labeling of TiO <sub>2</sub> precursor samples	Synthesis parameters					
		Solution mixing		Gel aging		Gel drying	
		Temperature, $T_{mixing}$ , °C	Time, $t_{mixing}$ , h	Temperature, $T_{aging}$ , °C	Time, $t_{aging}$ , h	Temperature, $T_{drying}$ , °C	Time, $t_{drying}$ , h
1	P-TiO <sub>2</sub> -1	20	2	20	5	80	2
2	P-TiO <sub>2</sub> -2	80	2	80	5	80	2

**Table 2.** List of investigated TiO<sub>2</sub> samples and conditions for their obtaining

Sample number	Labeling of TiO <sub>2</sub> samples	Type of precursor used (Table 1)	Calcination parameters of TiO <sub>2</sub> precursors			Note
			Temperature, $T_{calcination}$ , °C	Temperature rise rate, $v_{calcination}$ , °C/min	Isothermal aging time, $t_{calcination}$ , h	
1	TiO <sub>2</sub> -1	P-TiO <sub>2</sub> -1	500	5	4	samples synthesized by calcination of precursors
2	TiO <sub>2</sub> -2	P-TiO <sub>2</sub> -2				
3	TiO <sub>2</sub> -3	–	–	–	–	commercial (industrial) samples
4	TiO <sub>2</sub> -4					

### Evaluation of photocatalytic activity of TiO<sub>2</sub> samples

The photocatalytic activity of titanium dioxide samples was studied in a model photochemical reaction of oxidative destruction of methylene blue (MB), when aqueous suspensions of MB solution and TiO<sub>2</sub> powder were exposed to artificial ultraviolet and natural solar radiations. Two identical series of solutions with photocatalysts were the objects of study.

The weight ratio of TiO<sub>2</sub> and methylene blue in the suspensions was 50 : 1. The dye concentration in the solution was 10 mg/l. To destroy large agglomerates and evenly distribute the dispersed phase particles in the solution, ultrasonic dispersion of samples was performed for 10 min on the Bandelin Sonorex ultrasonic bath.

Ultraviolet light irradiated the first series of dye solutions with TiO<sub>2</sub> for 2 hours under constant stirring of suspensions on a magnetic stirrer. The radiation sources were two 25 W 254 nm UV lamps.

Solar radiation affected the second series of solutions with photocatalysts. Exposure of samples took place in the summer on the windowsill under natural daylight without using additional artificial light sources. The exposure time was 75 hours, namely 15 hours per day for 5 days.

During the study, aliquots of the solution were taken at certain intervals of exposure time to perform spectrophotometric measurements of the residual dye concentration. The sampling and measurement intervals were 15–30 minutes and 15 hours (1 day) for the first and sec-

ond series of samples, which were exposed to ultraviolet and solar radiation, respectively.

The selected samples were centrifuged for 15 min at 4000 rpm to separate the photocatalyst powder from the solution. The optical density of the solution (i.e. concentration of methylene blue) was measured at 664 nm relative to distilled water using the Shimadzu UV-1800 spectrophotometer. The measured absorption spectrum of aqueous solution of methylene blue, shown in Figure 1, led to the use of the above wavelength. The absorption spectrum of this dye had four characteristic peaks, including two peaks in the UV region at 246 nm and 292 nm, as well as two peaks in the visible region at 614 nm and 664 nm (the main maximum).

The formulas for calculating the residual relative concentration ( $\Delta C_t$ , rel. units) and the photocatalytic decomposition degree ( $\varphi_{\Delta C_t}$ , %) of methylene blue were:

$$\Delta C_t = \frac{C_t}{C_0}, \quad (2)$$

$$\begin{aligned} \varphi_{\Delta C_t} &= (1 - \Delta C_t) \cdot 100 \% = \\ &= \left(1 - \frac{C_t}{C_0}\right) \cdot 100 \% = \left(\frac{C_0 - C_t}{C_0}\right) \cdot 100 \%, \quad (3) \end{aligned}$$

where  $C_t$  is the optical density of MB solution after exposure to UV radiation or solar radiation during time ( $t$ ), rel. units (it characterizes the current dye concentration at time ( $t$ ), mmol/L);

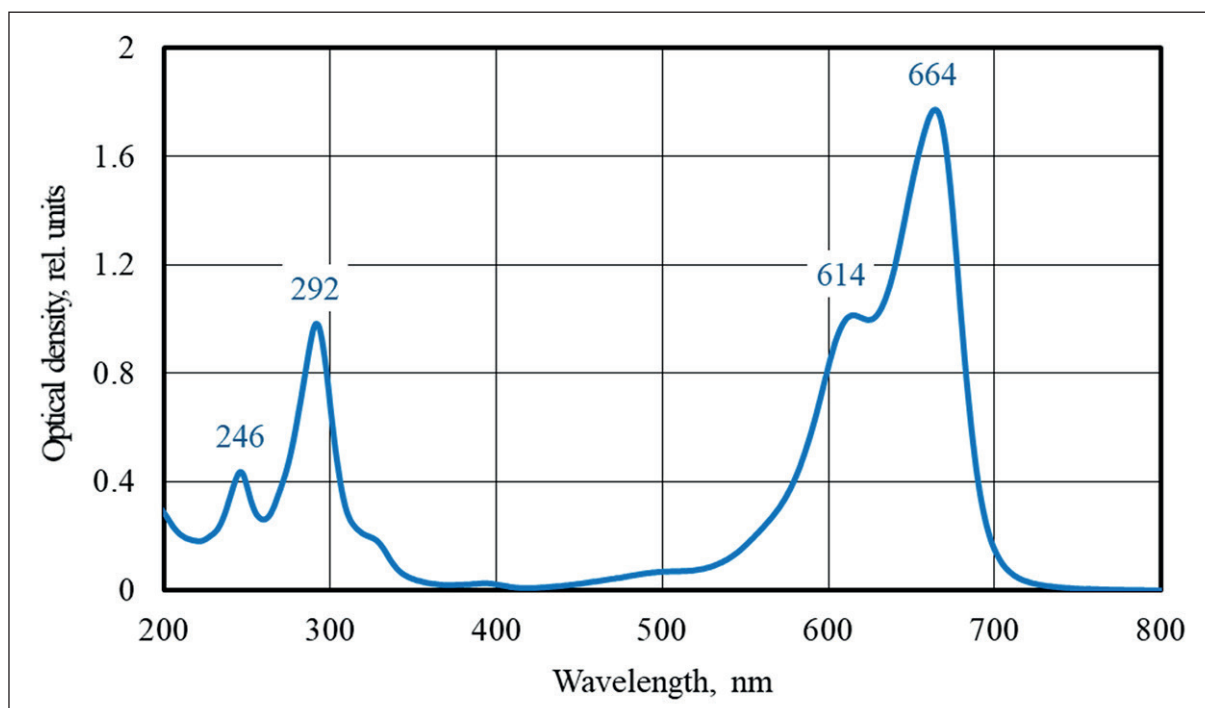


Fig. 1. Absorption spectrum of aqueous solution of methylene blue

$C_0$  is the initial optical density of MB solution, rel. units (it characterizes the initial dye concentration before exposure to UV light or sunlight ( $t_0 = 0$  minutes or  $t_0 = 0$  hours), mmol/L).

## RESULTS AND DISCUSSION

### Effects of synthesis conditions on structure parameters of $\text{TiO}_2$ precursors

Figure 2 shows the diffraction patterns of P-TiO<sub>2</sub>-1 and P-TiO<sub>2</sub>-2 samples of titanium dioxide precursors obtained under different synthesis conditions (see Table 1).

The study results showed that hydrated forms of titanium dioxide ( $\text{TiO}_2 \cdot n\text{H}_2\text{O}$ ), which have an X-ray amorphous structure, represented the phase composition of the P-TiO<sub>2</sub>-1 precursor synthesized at room temperature. The characteristic features of the diffraction pattern of this precursor, in particular, the complete absence of diffraction peaks and the presence of halos at  $2\theta = 20\text{--}40^\circ$  and  $2\theta = 40\text{--}55^\circ$  (Fig. 2), testified to this.

Compared with P-TiO<sub>2</sub>-1, increasing the synthesis temperature of the P-TiO<sub>2</sub>-2 sample from  $20^\circ\text{C}$  to  $80^\circ\text{C}$  led to the formation of crystalline phases of titanium(IV) oxide in the form of two polymorphic modifications, such as anatase and brookite. The diffraction peaks at  $2\theta$  of  $25.3^\circ$ ,  $37.9^\circ$ ,  $47.9^\circ$ ,  $54.5^\circ$ ,  $62.9^\circ$ , and  $69.5^\circ$  characterized the anatase phase with a tetragonal crystal lattice. The diffraction peaks located at  $2\theta$  of  $25.3^\circ$ ,  $30.8^\circ$ ,  $36.2^\circ$ ,  $42.4^\circ$ ,  $47.9^\circ$ , and  $54.5^\circ$  (Fig. 2) corresponded to the brookite phase related to orthorhombic syngony. The low intensity

and noticeable broadening of these peaks indicated the insignificant presence of X-ray amorphous component represented by titanium hydroxoforms in the P-TiO<sub>2</sub>-2 sample. By the nature of diffraction pattern profile, the X-ray amorphous phase content in this precursor was no more than 3–5%.

It is important to note that the most intense peaks at  $2\theta$  of  $25.3^\circ$ ,  $47.9^\circ$ , and  $54.5^\circ$  in the diffraction pattern of the P-TiO<sub>2</sub>-2 sample were a superposition of peaks from anatase and brookite. For this reason, the parameters of superposition-free diffraction peaks of these crystalline phases, in particular, those located at  $2\theta = 37.9^\circ$  for anatase and at  $2\theta = 30.8^\circ$  for brookite, acted as data for the quantitative phase analysis and evaluation of the crystallite (CSR) sizes using the Scherrer method.

According to the results of quantitative X-ray phase analysis, the crystallinity degree of the P-TiO<sub>2</sub>-2 sample structure was 97 % with the content of anatase and brookite in the phase composition equal to 81 wt. % and 16 wt. %, respectively, i.e. the ratio of anatase : brookite = 83.5 % : 16.5 %  $\approx$  5 : 1. The average size of coherent scattering regions (CSR) of anatase and brookite, calculated using formula (1), was 5.4 and 6.4 nm, respectively (Table 3).

Thus, in the experimental study, the nanocrystalline sample of titanium dioxide (P-TiO<sub>2</sub>-2), having the anatase/brookite structure, was obtained at low synthesis temperature ( $T = 80^\circ\text{C}$ ) and atmospheric pressure as a result of course of colloidal chemical processes in solutions. This low-temperature sol-gel method consisted of hydrolysis of titanium alkoxide in acidified water-alcoholic

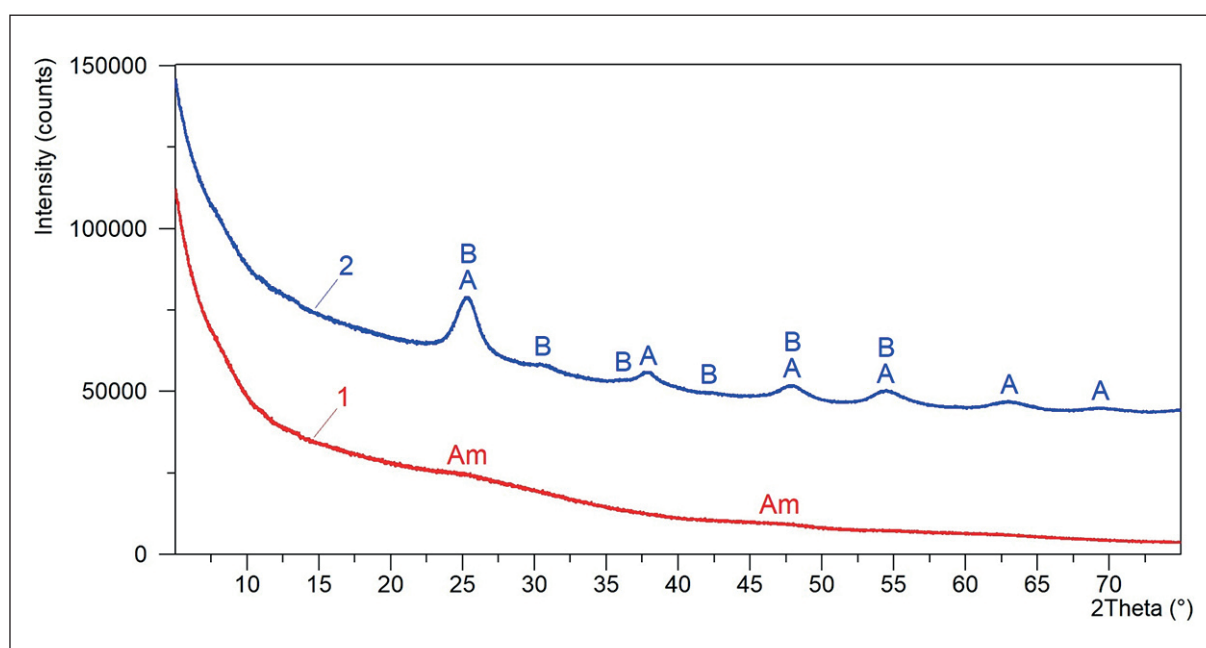


**Fig. 2.** Diffraction patterns of P-TiO<sub>2</sub>-1 (1) and P-TiO<sub>2</sub>-2 (2) samples of titanium dioxide precursors (see Table 1) with designated peaks of X-ray amorphous TiO<sub>2</sub> (Am), anatase (A), and brookite (B)

**Table 3.** Results of quantitative X-ray diffraction analysis of TiO<sub>2</sub> precursor samples (Table 1, Fig. 2)

Description of phases		Position of the main peaks <i>d</i> , Å (2θ, °)	Samples	
Type	Name		P-TiO <sub>2</sub> -1	P-TiO <sub>2</sub> -2
<i>Phase composition, wt. %</i>				
Amorphous phase	X-ray amorphous TiO <sub>2</sub>	halos corresponding to 4.4–2.3 Å (situated at 20–40°) and to 2.3–1.8 Å (at 40–52°) maximums in the area of 3.6 Å (25°) and 1.9 Å (47°)	100	3
Crystalline phases	anatase	3.52 Å, 2.37 Å, 1.90 Å, 1.68 Å, 1.48 Å, 1.35 Å (25.3°, 37.9°, 47.9°, 54.5°, 62.9°, 69.5°)	–	81
	brookite	3.52 Å, 2.90 Å, 2.48 Å, 2.13 Å, 1.90 Å, 1.68 Å (25.3°, 30.8°, 36.2°, 42.4°, 47.9°, 54.5°)	–	16
<i>Structure parameters of the samples</i>				
Crystallinity degree of the structure, %			0	97
Anatase/brookite ratio in the mixture of crystalline phases, %			–	83.5/16.5
Average CSR size of the crystalline phase, nm		anatase (peak at 2θ = 37.9°)	–	5.4
		brookite (peak at 2θ = 30.8°)	–	6.4

medium, exposure of the hydrolysis product at 80 °C, followed by washing and drying of the precipitate. It is known that the main advantages of low-temperature solution methods are the possibility of obtaining nanostructured titanium oxide-based photocatalysts without the use of ultrasonic treatment, autoclaving, and calcination of synthesis products at high temperatures ( $T \geq 400\text{--}500\text{ °C}$ ) [35, 40, 54].

### Phase composition of TiO<sub>2</sub> samples

Figure 3 shows the diffraction patterns of TiO<sub>2</sub>-1 and TiO<sub>2</sub>-2 titanium dioxide samples synthesized by calcination of the P-TiO<sub>2</sub>-1 and P-TiO<sub>2</sub>-2 precursors (see Table 1 and Fig. 2), as well as the diffraction patterns of TiO<sub>2</sub>-3 and TiO<sub>2</sub>-4 control industrial samples (see Table 2).

It was found that the phase composition of the studied samples included from one to three polymorphic modifications of TiO<sub>2</sub>, namely anatase, brookite, and rutile. The diffraction peaks located at 2θ of 25.3°, 37.8°, 48.1°, 53.9°, 55.1°, 62.7°, 68.8°, 70.3°, and 2θ of 27.4°, 36.1°, 39.2°, 41.2°, 44.0°, 54.3°, 56.6°, 62.7°, 64.0°, 69.0°, 69.8° (Table 4) in the diffraction patterns (Fig. 3) respectively characterized the anatase and rutile phases with tetragonal crystal lattices. The diffraction peaks situated at 2θ of 25.3°, 30.8°, 36.1°, 48.1°, 53.9°, and 55.1° cor-

responded to the brookite phase related to orthorhombic syngony.

It was determined that the TiO<sub>2</sub>-1 and TiO<sub>2</sub>-3 samples contained only one crystalline phase in the form of anatase and rutile, respectively. The structure of the TiO<sub>2</sub>-4 sample was two-phase and consisted predominantly of rutile (97 wt. %) with inclusion of anatase (3 wt. %). The TiO<sub>2</sub>-2 sample included three phases as a mixture of anatase, brookite, and rutile with the weight component ratio of 67 % : 13 % : 20 % ≈ 5.2 : 1 : 1.5 (Table 4).

The effects of the synthesis temperature of TiO<sub>2</sub> precursors on the phase composition of their calcination products were analyzed. It is known that thermal treatment leads to the ordering of the precursor structure due to the occurrence of olation-oxolation processes that promote the substance transition from X-ray amorphous to crystalline state. It was found that calcination of the P-TiO<sub>2</sub>-1 precursor at 500 °C resulted to the formation of the anatase phase from X-ray amorphous TiO<sub>2</sub> (see Figs. 2 and 3). At the same time, such thermal treatment of the P-TiO<sub>2</sub>-2 precursor contributed to the occurrence of three parallel crystallization processes, which gave rise to the phase transitions from X-ray amorphous TiO<sub>2</sub> to anatase, from anatase to rutile, and from brookite to rutile.

Thus, the obtained experimental data showed that the increase in the precursor synthesis temperature from

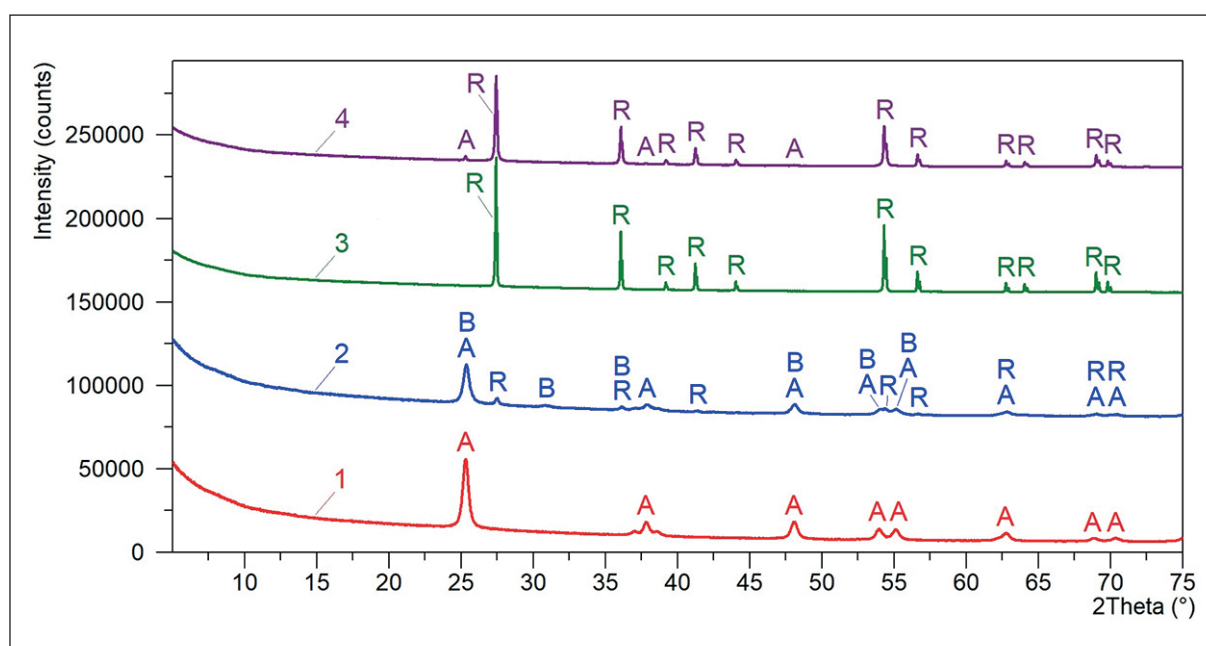


**Fig. 3.** Diffraction patterns of TiO<sub>2</sub>-1 (1), TiO<sub>2</sub>-2 (2), TiO<sub>2</sub>-3 (3), and TiO<sub>2</sub>-4 (4) samples of titanium dioxide (see Table 2) with designated peaks of anatase (A), brookite (B), and rutile (R)

20 °C (for P-TiO<sub>2</sub>-1) to 80 °C (for P-TiO<sub>2</sub>-2) led to a decrease in the initial crystallization temperature of rutile. At the same time, the differences in the phase composition of the TiO<sub>2</sub>-2 and P-TiO<sub>2</sub>-2 samples indicated that the crystallization of rutile occurred primarily due to anatase and to a lesser extent due to brookite.

The structure crystallinity of TiO<sub>2</sub> samples was evaluated during the study. The synthesized TiO<sub>2</sub>-1 and TiO<sub>2</sub>-2 samples had a nanocrystalline structure, as evidenced by the reduced intensity and noticeable broadening of the diffraction peaks of the crystalline phases in the diffraction patterns. The average CSR size of the anatase, brookite, and rutile phases, calculated using the Scherrer formula (1), for the TiO<sub>2</sub>-1 and TiO<sub>2</sub>-2 samples was 13.0–17.3 nm, 13.4 nm, and 31.3 nm, respectively. Thus, the P-TiO<sub>2</sub>-2 precursor calcination at 500 °C resulted in the increase of the anatase crystallite size, estimated by the peak at 2θ = 37.8–37.9°, from 5.4 nm to 13.0 nm, i.e. by 2.4 times (see Tables 3 and 4).

The industrial TiO<sub>2</sub>-3 and TiO<sub>2</sub>-4 samples had larger crystallite sizes. The average CSR sizes of the anatase and rutile phases for these control samples were 38.0–50.6 nm and 53.8–86.1 nm, respectively, which was 2.2–3.9 times and 1.7–2.8 times higher than the similar parameters of the synthesized TiO<sub>2</sub>-1 and TiO<sub>2</sub>-2 samples (Table 4).

### Photocatalytic activity of TiO<sub>2</sub> samples

It is known [55] that the rate of a dye solution discoloration during photocatalysis is determined by the combined action of several basic processes, such as:

1. Dye photodegradation in the liquid phase.
2. Dye adsorption on the photocatalyst surface.
3. Photocatalytic decomposition of dye molecules adsorbed on the surface of photocatalyst particles.

Processes 2 and 3 are sequential, while the dye photodegradation in the liquid phase proceeds independently and simultaneously with processes 2 and 3.

Figure 4 shows the kinetic curves of methylene blue (MB) photodegradation in solution under exposure conditions of ultraviolet radiation (a) and solar radiation (b) in the absence and presence of titanium oxide-based photocatalysts such as TiO<sub>2</sub>-1, TiO<sub>2</sub>-2, TiO<sub>2</sub>-3, and TiO<sub>2</sub>-4. The kinetic curves show the change in relative dye concentration in solution ( $\Delta C_t$ ), calculated using the formula (2), during ultraviolet irradiation for 120 minutes (Fig. 4(a)), as well as under exposure conditions to sunlight (natural daylight) for 75 hours (Fig. 4(b)).

The study results showed that the concentration of methylene blue in the solution decreased exponentially under ultraviolet radiation. The rate of the photochemical reaction of dye decomposition was highest in the first 15–30 minutes of UV light irradiation (Fig. 4(a)). The degree of MB degradation in the solution ( $\varphi_{\Delta C_t}$ , see formula (3)) in the absence of photocatalyst was  $\varphi_{\Delta C_t, 120 \text{ min}} = 11.0\%$  after 120 minutes of UV exposure. When using control TiO<sub>2</sub>-3 and TiO<sub>2</sub>-4 samples, the dye photodecomposed to the specified degree (11%) in less than 30 minutes of UV exposure, while the  $\varphi_{\Delta C_t, 120 \text{ min}}$  parameter increased by 3.8 times and 5.2 times to the level of 42.2% and 57.1%, respectively.

The presence of photocatalysts based on synthesized TiO<sub>2</sub>-1 and TiO<sub>2</sub>-2 samples in the solution resulted in

**Table 4.** Results of quantitative X-ray diffraction analysis of TiO<sub>2</sub> samples (Table 2, Fig. 3)

Description of phases		Position of the main peaks <i>d</i> , Å (2θ, °)	Samples			
Type	Name		TiO <sub>2</sub> -1	TiO <sub>2</sub> -2	TiO <sub>2</sub> -3	TiO <sub>2</sub> -4
<i>Phase composition, wt. %</i>						
Crystalline phases	anatase	3.52 Å, 2.38 Å, 1.89 Å, 1.70 Å, 1.67 Å, 1.48 Å, 1.36 Å, 1.34 Å (25.3°, 37.8°, 48.1°, 53.9°, 55.1°, 62.7°, 68.8°, 70.3°)	100	67	–	3
	brookite	3.52 Å, 2.90 Å, 2.49 Å, 1.89 Å, 1.70 Å, 1.67 Å (25.3°, 30.8°, 36.1°, 48.1°, 53.9°, 55.1°)	–	13	–	–
	rutile	3.25 Å, 2.49 Å, 2.30 Å, 2.19 Å, 2.06 Å, 1.69 Å, 1.63 Å, 1.48 Å, 1.45 Å, 1.36 Å, 1.35 Å (27.4°, 36.1°, 39.2°, 41.2°, 44.0°, 54.3°, 56.6°, 62.7°, 64.0°, 69.0°, 69.8°)	–	20	100	97
<i>Average CSR size of the crystalline phases, nm</i>						
anatase		peak at 2θ = 25.3°	17.3	13.0	–	50.6
		peak at 2θ = 37.8°	17.2	13.0	–	38.0
brookite		peak at 2θ = 30.8°	–	13.4	–	–
rutile		peak at 2θ = 27.4°	–	31.3	86.1	53.8

a significant increase in the efficiency of dye photodegradation under UV radiation. In particular, when using these photocatalysts, the time to achieve the destruction level of methylene blue  $\varphi_{\Delta C_t} = 11\%$ , corresponding to 120-minute photolysis of the dye, was 3–5 minutes. At the same time, the decomposition degree of methylene blue after  $t = 120$  minutes of UV irradiation was 99.7% and 97.3% in solutions with TiO<sub>2</sub>-1 and TiO<sub>2</sub>-2, respectively (Fig. 4(a)). It was 8.8–9.1 times and 1.7–2.4 times higher than the  $\varphi_{\Delta C_{120 \text{ min}}}$  values recorded (1) during the MB photolysis in solution without photocatalysts and (2) during the dye photocatalytic decomposition in the presence of TiO<sub>2</sub>-3 and TiO<sub>2</sub>-4 control samples.

The efficiency of titanium oxide-based photocatalysts decreased significantly under conditions of sunlight exposure. It was revealed that the degradation rate of methylene blue was highest in the first 15 hours of natural light (first day of exposure) (Fig. 4 (b)). The decomposition degree of the dye in the solution without photocatalysts after  $t = 75$  hours of exposure to daylight was  $\varphi_{\Delta C_{75 \text{ hours}}} = 88.2\%$ . The presence of TiO<sub>2</sub>-3 and TiO<sub>2</sub>-4 powders in the solution only slightly increased the  $\varphi_{\Delta C_{75 \text{ hours}}}$  value, to the level of 91.0% and 92.2%, respectively. The photodestruction degree of methylene blue after  $t = 75$  hours of exposure to solar radiation was 99.5% and 99.7% when using the synthesized TiO<sub>2</sub>-1 and TiO<sub>2</sub>-2 photocatalysts, respectively (Fig. 4(b)). In addition, the time to achieve the level of MB degradation  $\varphi_{\Delta C_t} = 88\%$ , characteristic of 75-hour photolysis of the dye, for solutions with TiO<sub>2</sub>-1 and TiO<sub>2</sub>-2

was reduced to 50–55 hours, which was 15–22 hours less than for the TiO<sub>2</sub>-3 and TiO<sub>2</sub>-4 control samples.

It is known that the Langmuir–Hinshelwood model often describes the kinetics of photolysis and photocatalytic degradation of dye molecules in an aqueous medium, while the linearized integral forms of pseudo-first (4) or pseudo-second (5) order reaction equations usually approximate experimental data [56, 57]:

$$-\ln\left(\frac{C_t}{C_0}\right) = k_1 \cdot t, \quad (4)$$

$$\frac{1}{C_t} - \frac{1}{C_0} = k_2 \cdot t, \quad (5)$$

there  $C_0$  and  $C_t$  are the initial and current concentrations of the dye in aqueous solution (the same as in formulas (2) and (3)), mmol/L;

$t$  is the time of photochemical reaction, such as photolysis or photocatalytic decomposition of the dye, corresponding to the duration of exposure to UV radiation or solar radiation, min or h;

$k_1$  is the rate constant of photochemical reaction, such as photolysis or photocatalytic decomposition of the dye, in the linearized pseudo-first order kinetic equation (4), min<sup>-1</sup> or h<sup>-1</sup>;

$k_2$  is the rate constant of photochemical reaction, such as photolysis or photocatalytic decomposition of the dye, in the linearized pseudo-second order kinetic equation (5), L/(mmol·min) or L/(mmol·h).

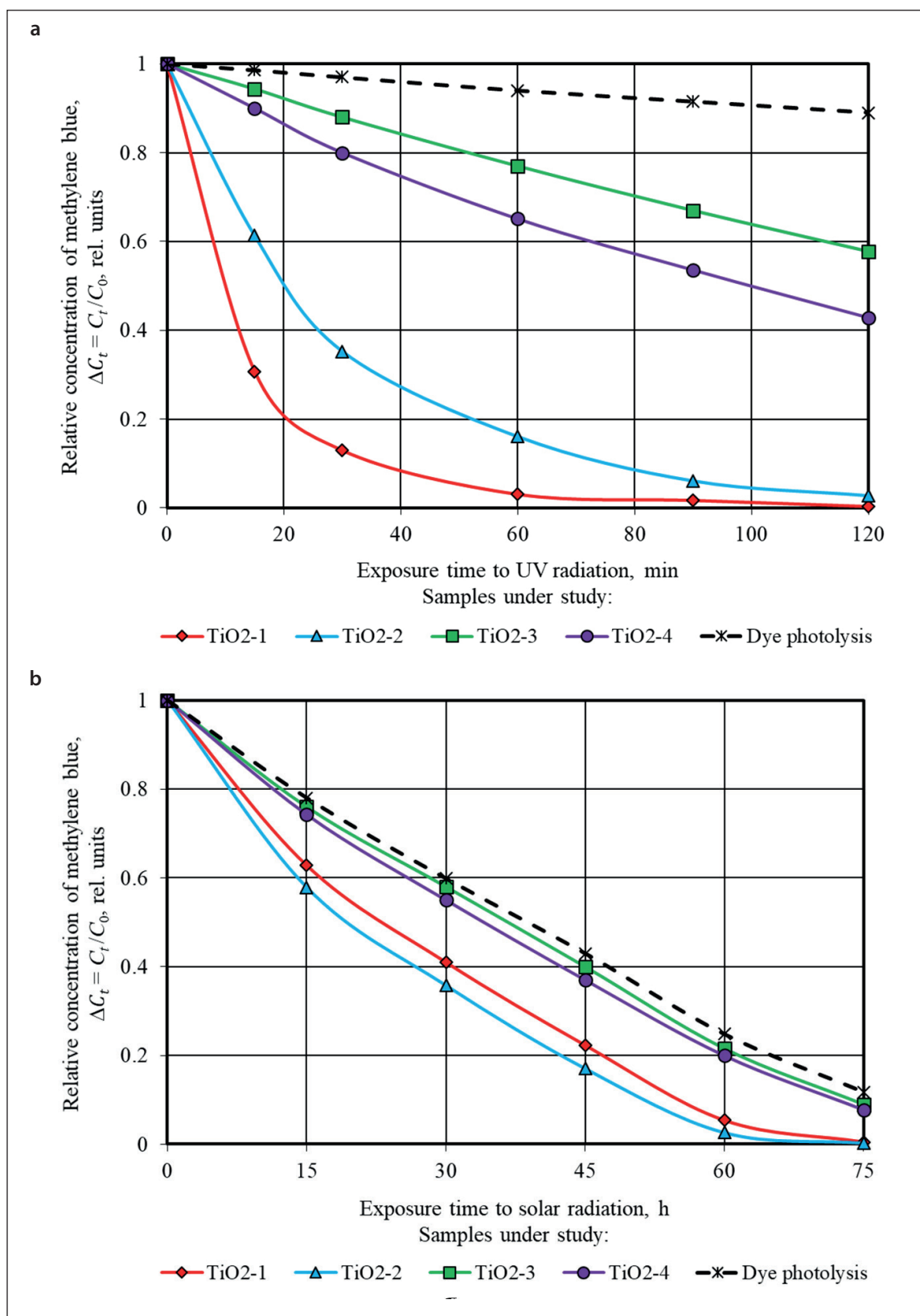


**Fig. 4.** Kinetic curves of methylene blue photodegradation in solution under UV radiation (a) and solar radiation (b) in the absence of photocatalysts (black dotted curve characterizes to MB photolysis) and in the presence of TiO<sub>2</sub> samples (colored solid curves characterize to MB photocatalytic decomposition processes)

Figures 5 and 6 show graphs describing the kinetics of photolysis and photocatalytic degradation of methylene blue in solution under UV light irradiation and sunlight irradiation using pseudo-first order and pseudo-second order

reaction equations. The angle of inclination of the linear dependences allowed to identify the rate constant values of the corresponding photochemical reactions occurring in the absence and in the presence of photocatalysts.

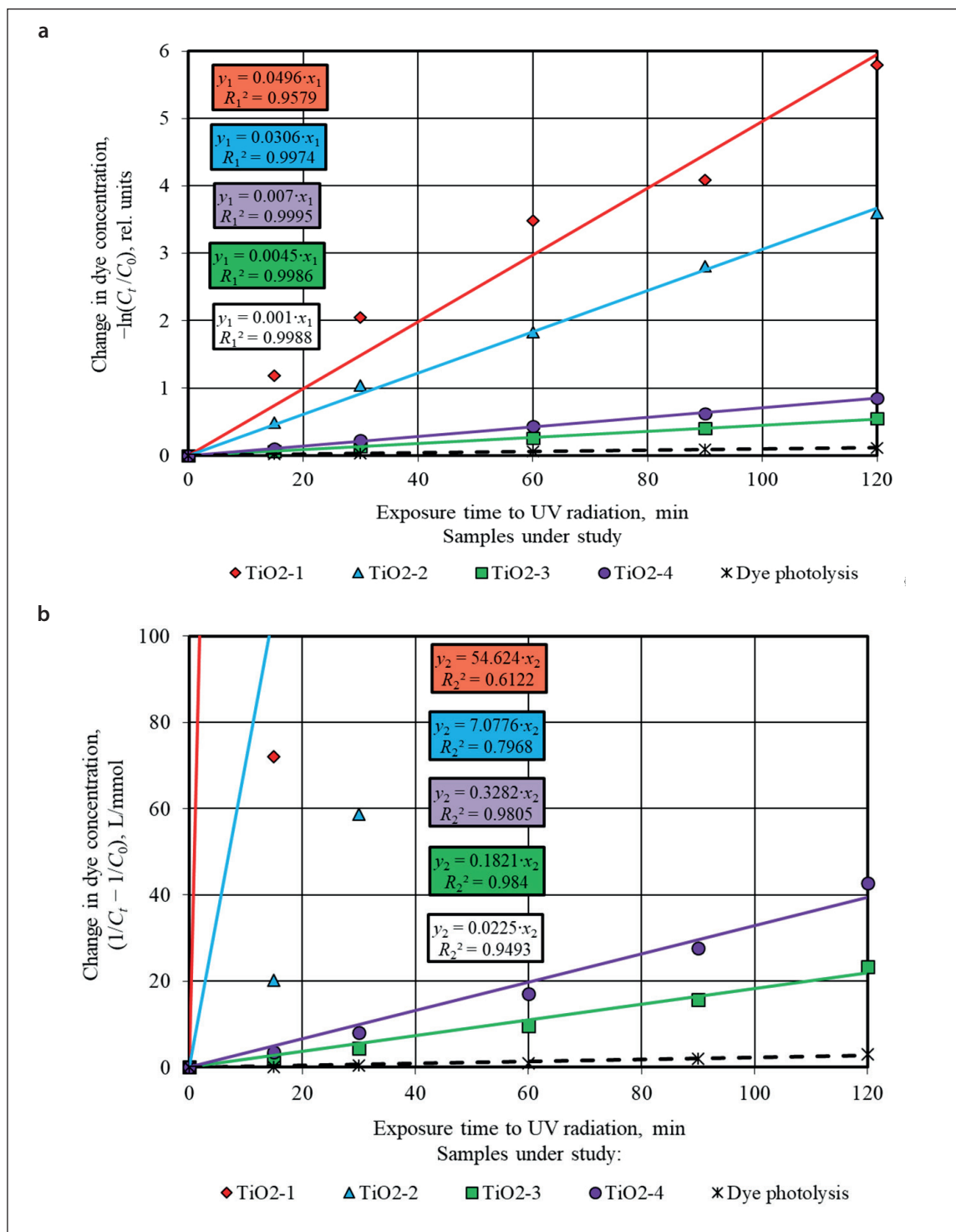


**Fig. 5.** Description of the methylene blue photodecomposition kinetics in solution under UV radiation in the absence (black dotted lines) and in the presence of photocatalysts based on  $TiO_2$  (colored solid lines) in the coordinates of pseudo-first order (a) and pseudo-second order (b) kinetic models

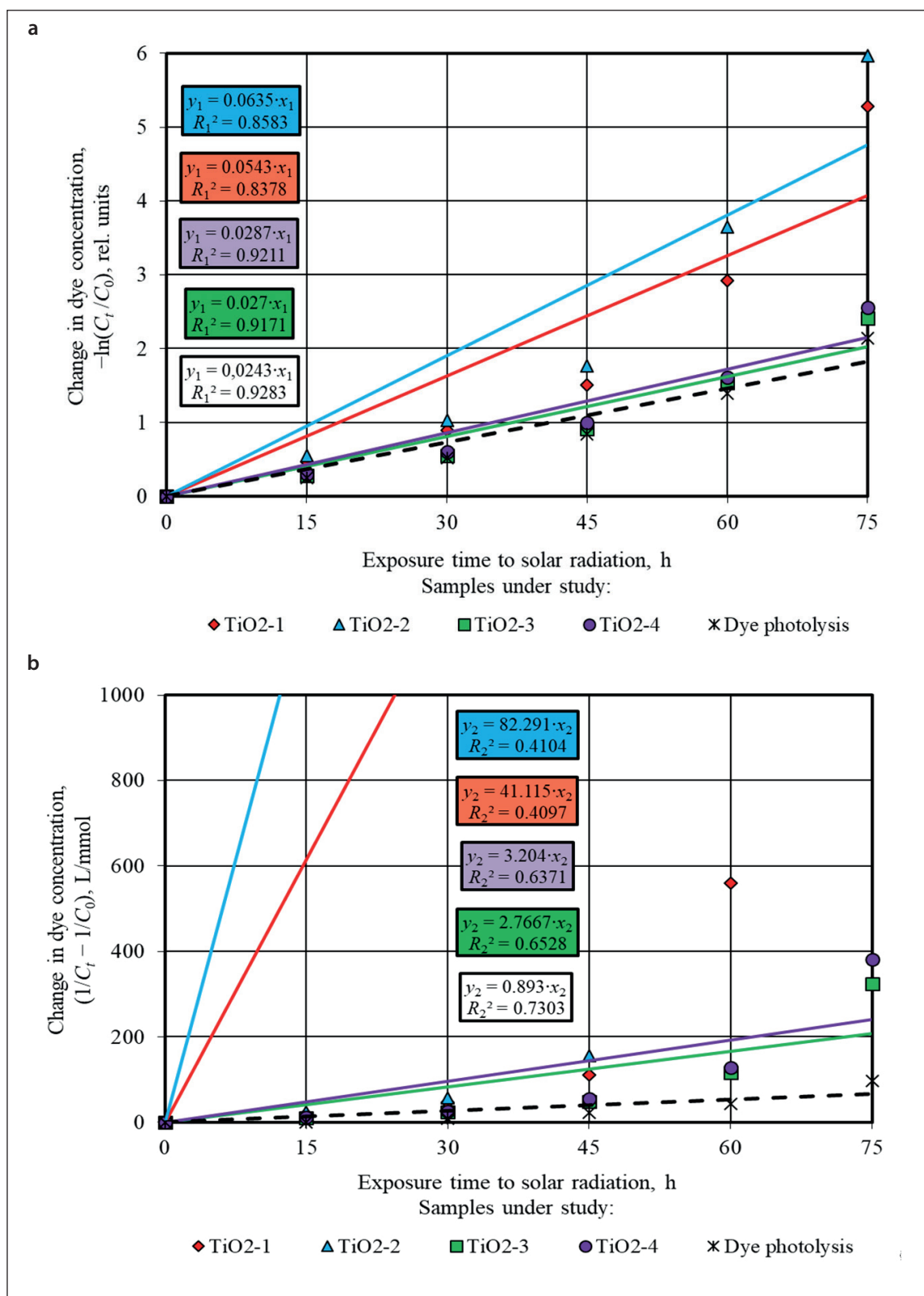


**Fig. 6.** Description of the methylene blue photodecomposition kinetics in solution under solar radiation in the absence (black dotted lines) and in the presence of photocatalysts based on  $\text{TiO}_2$  (colored solid lines) in the coordinates of pseudo-first order (a) and pseudo-second order (b) kinetic models

It was established that the pseudo-first order equations most adequately approximate the experimental data obtained during the study of photochemical reactions under UV radiation and solar radiation. Higher values of the determination coefficients in models (4) compared to pseudo-second order models (5), namely  $R_1 = 0.9579–0.9995 > R_2 = 0.6122–0.984$  (UV light, Fig. 5) and  $R_1 = 0.8378–0.9283 > R_2 = 0.4097–0.7303$  (sunlight, Fig. 6), testify to this.

It is known [57, 58] that heterogeneous reactions have two possible modes of course depending on the limiting stage, in particular, kinetic mode and diffusion mode characterized by the limiting contribution of chemical reaction or diffusion, respectively. A more accurate description of the experimental data by the pseudo-second order kinetic model indicates the limiting contribution of the chemical reaction to the heterogeneous process. The conformity of the process kinetics to the pseudo-first order model suggests that the diffusion stage limits the heterogeneous reaction. Thus, the obtained experimental data showed that the photodegradation of methylene blue in solution under UV radiation and solar radiation with the participation of TiO<sub>2</sub>-1, TiO<sub>2</sub>-2, TiO<sub>2</sub>-3, and TiO<sub>2</sub>-4 samples proceeded in the diffusion mode due to the correspondence to the pseudo-first order model (4). Dye adsorption on the surface of titanium oxide-based photocatalysts limited these photocatalytic processes.

The study results showed that the presence of titanium dioxide powders in the solution significantly intensified the process of methylene blue decomposition under UV light irradiation. The values of the rate constants of pseudo-first order reactions for photocatalytic processes were  $k_1 = 0.0045–0.0496 \text{ min}^{-1}$ , which was 4.5–49.6 times higher than in the dye photolysis without titanium oxide-based photocatalysts ( $k_1 = 0.001 \text{ min}^{-1}$ ) (Fig. 5(a)).

The photoactivity of the studied TiO<sub>2</sub> samples markedly decreased under the conditions of solar radiation exposure (Fig. 6(a)), which was evidenced by the convergence of the values of the rate constants of photocatalytic reactions ( $k_1 = 0.027–0.0635 \text{ h}^{-1}$ ) and dye photolysis ( $k_1 = 0.0243 \text{ h}^{-1}$ ).

According to Fig. 4, 5, and 6, the synthesized TiO<sub>2</sub>-1 and TiO<sub>2</sub>-2 samples had higher photocatalytic activity compared to the TiO<sub>2</sub>-3 and TiO<sub>2</sub>-4 control industrial samples, regardless of the exposure conditions, namely UV radiation or solar radiation.

The phase composition noticeably influenced the efficiency of titanium oxide-based photocatalysts. It was revealed that polymorphic modifications of TiO<sub>2</sub> had multidirectional effects on the functional characteristics of the material, in particular, an increase in the content of anatase and rutile led to an increase and decrease in the photoactivity of TiO<sub>2</sub> samples, respectively (Fig. 7). The single-phase TiO<sub>2</sub>-1 sample of anatase modification was the most effective under UV irradiation, while the three-

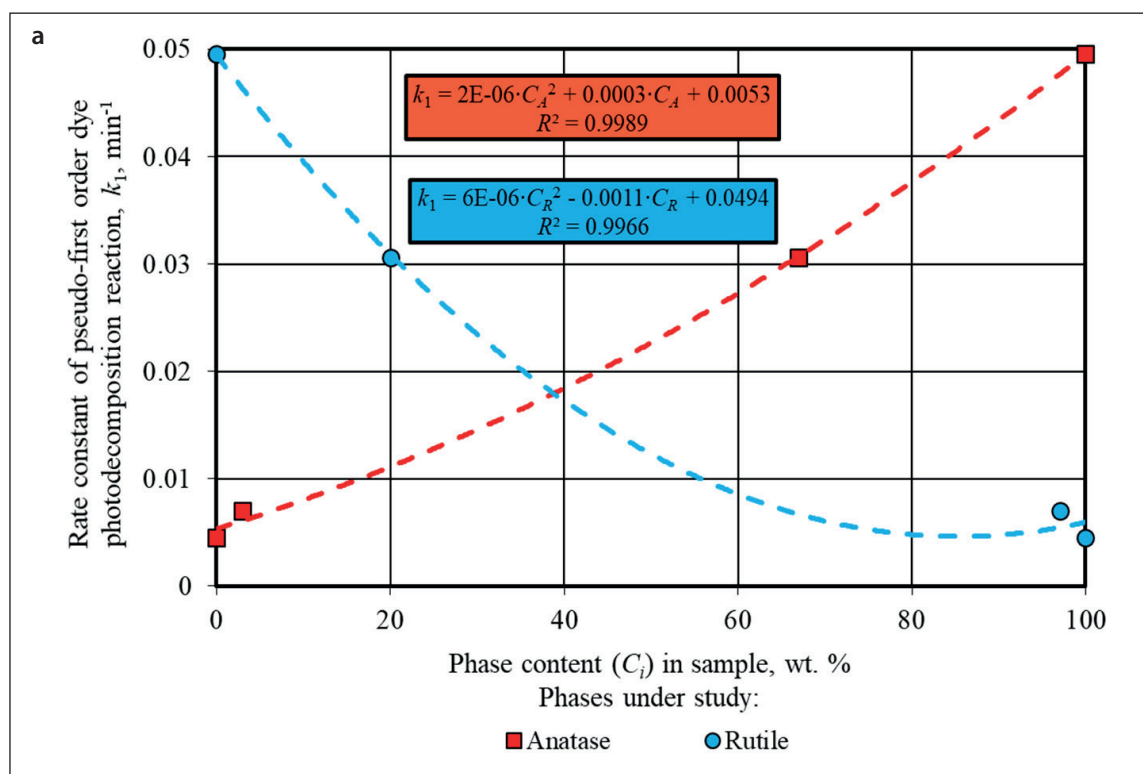


**Fig. 7.** Effects of anatase and rutile content in phase composition on photocatalytic activity of titanium dioxide in methylene blue solution under ultraviolet radiation (a) and solar radiation (b)

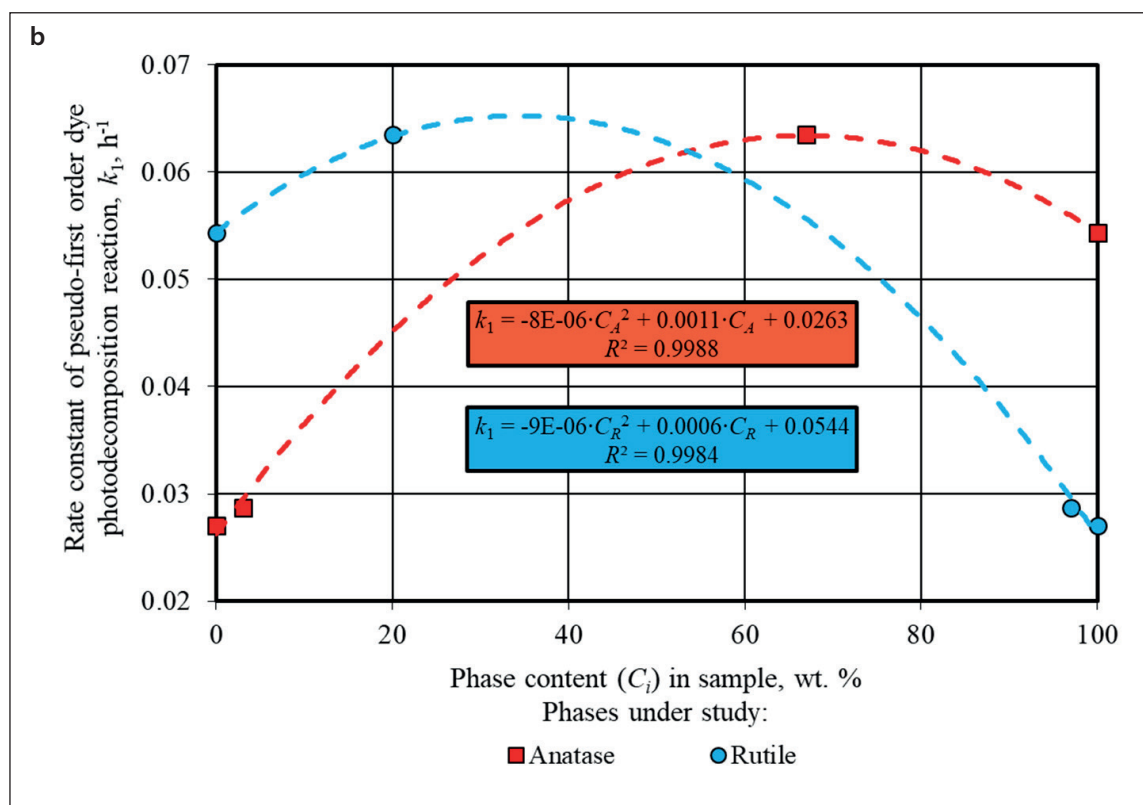


Fig. 7. The End

phase TiO<sub>2</sub>-2 sample with the ratio of anatase : brookite : rutile = 67% : 13% : 20%  $\approx$  5,2 : 1 : 1,5 (Table 4) had the highest activity under daylight exposure. At the same time, according to Fig. 7, the photoactivity of heterophase samples under solar was higher in comparison with the TiO<sub>2</sub>-1 sample when the content of anatase in the mixture of crystalline phases was at least 40–50%, i.e. when this phase prevailed in the material composition.

The obtained experimental data were consistent with the results of studies by other authors. In particular, the papers [35, 39, 40] showed that the combination of two or three polymorphic modifications of TiO<sub>2</sub> in the structure, in particular, anatase/rutile, anatase/brookite, anatase/brookite/rutile with anatase predominating, made it possible to increase the photocatalytic activity of the material compared to single-phase titanium oxide photocatalysts by reducing the recombination rate of photoinduced charge carriers.

## CONCLUSION

The following scientific results were obtained in the paper:

1. The effects of synthesis conditions on the structure parameters of TiO<sub>2</sub> precursors obtained by hydrolysis of titanium alkoxide in acidified water-alcoholic medium were established.

2. The phase composition features were determined for four titanium(IV) oxide samples, namely two industrial samples and two samples synthesized by calcination of TiO<sub>2</sub> precursors at 500 °C.

3. The kinetics of photodecomposition process of methylene blue in solution was disclosed under conditions of exposure to ultraviolet radiation and solar radiation in the absence and presence of titanium oxide-based photocatalysts. The most effective TiO<sub>2</sub> samples under the specified exposure conditions were determined.

4. The effects of phase composition on the photocatalytic activity of titanium dioxide samples were revealed under conditions of exposure to artificial ultraviolet light and natural daylight.

5. The interrelations and regularities were established between the synthesis conditions, phase composition and photoactivity of TiO<sub>2</sub>, which made it possible to optimize the prescription and technological parameters for obtaining effective titanium oxide-based photocatalysts for self-cleaning concrete.

The results of the experimental study showed the possibility of obtaining the nanocrystalline sample of titanium(IV) oxide with anatase/brookite structure at low synthesis temperature ( $T = 80$  °C) and atmospheric pressure as a result of course of colloidal-chemical processes in solutions. It was revealed that a decrease in the synthesis temperature, including the gel aging tempera-

ture, from 80 to 20 °C led to the transition of TiO<sub>2</sub> from the nanocrystalline to X-ray amorphous state.

The phase composition noticeably influenced the efficiency of titanium oxide-based photocatalysts. It was found that polymorphic modifications of TiO<sub>2</sub> had multidirectional effects on its functional characteristics, in particular, an increase in the content of anatase and rutile led to an increase and decrease in the photoactivity of titanium dioxide samples, respectively. The single-phase sample with anatase structure was the most effective under UV irradiation, while the three-phase sample with the ratio of anatase : brookite : rutile = 67% : 13% : 20% ≈ 5,2 : 1 : 1,5 had the highest activity under daylight exposure.

The photocatalyst composition, including several polymorphs of TiO<sub>2</sub> with a predominance of anatase form (more than 50%), allowed to achieve a synergistic effect of increasing the photocatalytic activity of titanium dioxide under conditions of solar radiation due to the formation of type-II semiconductor heterojunctions in multiphase composite. Heterostructures made it possible to improve the spatial separation of charge carriers and to reduce the recombination rate of photogenerated electron-hole pairs. Thus, the obtained results indicated the possibility of improving the functional characteristics of titanium oxide-based additives for self-cleaning concrete due to the targeted regulation of their phase composition by optimizing the synthesis parameters of photocatalytic modifiers.

## REFERENCES

1. O'Hegarty R., Kinnane O., Newell J., West R. High performance, low carbon concrete for building cladding applications. *Journal of Building Engineering*. 2021; 43: 102566. <https://doi.org/10.1016/j.jobbe.2021.102566>
2. Mukhametrakhimov R.Kh., Garafiev A.M., Aleksandrova O.V., Bulgakov B.I. Structure and properties of modified shungite concrete during electrode heating. *Construction Materials and Products*. 2023; 6(6): 1. <https://doi.org/10.58224/2618-7183-2023-6-6-1>
3. Sifan M., Nagaratnam B., Thamboo J., Poologanathan K., Corradi M. Development and prospectives of lightweight high strength concrete using lightweight aggregates. *Construction and Building Materials*. 2023; 362: 129628. <https://doi.org/10.1016/j.conbuildmat.2022.129628>
4. Rassokhin A.S., Ponomarev A.N., Figovsky O.L. Silica fumes of different types for high-performance fine-grained concrete. *Magazine of Civil Engineering*. 2018; 78: 151–160. <https://doi.org/10.18720/MCE.78.12>
5. Carballosa P., García Calvo J.L., Revuelta D., Sánchez J.J., Gutiérrez J.P. Influence of cement and expansive additive types in the performance of self-stressing and self-compacting concretes for structural elements. *Construction and Building Materials*. 2015; 93: 223–229 <https://doi.org/10.1016/j.conbuildmat.2015.05.113>
6. Kaprielov S.S., Sheinfeld A.V., Kardumyan G.S., Chilin I.A. About selection of compositions of high-quality concretes with organic-mineral modifiers. *Construction Materials*. 2017; 12: 58–63. (In Russ.)
7. Nizina T.A., Balykov A.S., Korovkin D.I., Volodin V.V. Physical and mechanical properties of modified fine-grained fibre-reinforced concretes containing carbon nanostructures. *International Journal of Nanotechnology*. 2019; 16: 496–509. <https://doi.org/10.1504/IJNT.2019.106621>
8. Pukhareno Yu.V., Khrenov G.M., Klyuev S.V., Khezhev T.A. Eshanzada S.M. Design of steel fiber-reinforced concrete for slip forming. *Construction Materials and Products*. 2024; 7(5): 2. <https://doi.org/10.58224/2618-7183-2024-7-5-2>
9. Nizina T.A., Ponomarev A.N., Balykov A.S., Korovkin D.I. Multicriteria optimisation of the formulation of modified fine-grained fibre concretes containing carbon nanostructures. *International Journal of Nanotechnology*. 2018; 15: 333–346. <https://doi.org/10.1504/IJNT.2018.094790>
10. Ge L., Zhang Y., Sayed U., Li H. Study on properties of basalt fiber reinforcing reactive powder concrete under different curing conditions. *Journal of Materials Research and Technology*. 2023; 27: 5739–5751. <https://doi.org/10.1016/j.jmrt.2023.10.289>
11. Tolstoy A.D., Lesovik V.S., Zagorodnyuk L.Kh., Kovaleva I.A. Powder concretes with technogenic materials. *Proceedings of Moscow State University of Civil Engineering*. 2015; 11: 101–109. (In Russ.)
12. Wang W., Wu J., Yang W., Wang S., Wu H., Zhu Z., Wang L., Ding Q., Wang H., Zhou X. Towards low-temperature shrinkable synthetic fibers for internally self-prestressing concrete. *Journal of Building Engineering*. 2023; 73: 106769. <https://doi.org/10.1016/j.jobbe.2023.106769>
13. Dhahir M.K., Marx S. Development of expansive concrete for chemical prestressing applications. *Case Studies in Construction Materials*. 2023; 19: e02611. <https://doi.org/10.1016/j.cscm.2023.e02611>

14. Kapeluszna E., Chrabąszcz K. Mutual compatibility of superplasticizers (PC, SNF), grinding aids (TEA, glycol) and  $C_3A$  in Portland cement systems – Hydration, rheology, physical properties and air void characteristics. *Construction and Building Materials*. 2023; 373: 130877. <https://doi.org/10.1016/j.conbuildmat.2023.130877>
15. Lesovik V.S., Popov D.Y., Fediuk R.S., Sabri M.M., Vavrenyuk S.V., Liseitsev Yu.L. Shrinkage of ultra-high performance concrete with superabsorbent polymers. *Magazine of Civil Engineering*. 2023; 121: 12108. <https://doi.org/10.34910/MCE.121.8>
16. Shcherban' E.M., Stel'makh S.A., Mailyan L.R., Beskopylny A.N., Smolyanichenko A.S., Chernil'nik A.A., Elshaeva D.M., Beskopylny N.A. Structure and Properties of Variotropic Concrete Combined Modified with Nano- and Micro-silica. *Construction Materials and Products*. 2024; 7(2): 3. <https://doi.org/10.58224/2618-7183-2024-7-2-3>
17. Balykov A.S., Nizina T.A., Kyashkin V.M., Volodin S.V. Prescription and technological efficiency of sedimentary rocks of various composition and genesis in cement systems. *Nanotechnologies in Construction*. 2022; 14(1): 53–61. <https://doi.org/10.15828/2075-8545-2022-14-1-53-61>
18. Strokova V.V., Markova I.Yu., Markov A.Yu., Stepanenko M.A., Nerovnaya S.V., Bondarenko D.O., Botsman L.N. Properties of a composite cement binder using fuel ashes. *Key Engineering Materials*. 2022; 909: 184–190. <https://doi.org/10.4028/p-tm4y4j>
19. Balykov A.S., Nizina T.A., Volodin V.V., Kyashkin V.M. Effects of Calcination Temperature and Time on the Physical-Chemical Efficiency of Thermally Activated Clays in Cement Systems. *Materials Science Forum*. 2021; 1017: 61–70. <https://doi.org/10.4028/www.scientific.net/MSF.1017.61>
20. Balykov A.S., Nizina T.A., Volodin S.V. Optimization of technological parameters for obtaining mineral additives based on calcined clays and carbonate rocks for cement systems. *Nanotechnologies in Construction*. 2022; 14(2): 145–155. <https://doi.org/10.15828/2075-8545-2022-14-2-145-155>
21. Klyuev S., Ayubov N., Ageeva M., Fomina, E., Klyuev A., Usanova K., Shorstova E. Fine-grained concrete properties in depending on carbon black additive introducing methods. *Journal of Materials Research and Technology*. 2024; 32: 1996–2004. <https://doi.org/10.1016/j.jmrt.2024.08.052>
22. Amor F., Baudys M., Racova Z., Scheinherrová L., Ingrisova L., Hajek P. Contribution of  $TiO_2$  and  $ZnO$  nanoparticles to the hydration of Portland cement and photocatalytic properties of High Performance Concrete. *Case Studies in Construction Materials*. 2022; 16: e00965. <https://doi.org/10.1016/j.cscm.2022.e00965>
23. Janczarek M., Klapiszewski Ł., Jędrzejczak P., Klapiszewska I., Śłosarczyk A., Jesionowski T. Progress of functionalized  $TiO_2$ -based nanomaterials in the construction industry: A comprehensive review. *Chemical Engineering Journal*. 2022; 430(3): 132062. <https://doi.org/10.1016/j.cej.2021.132062>
24. Yang L., Hakki A., Wang F., Macphee D.E. Photocatalyst efficiencies in concrete technology: The effect of photocatalyst placement. *Applied Catalysis B: Environmental*. 2018; 222: 200–208. <https://doi.org/10.1016/j.apcatb.2017.10.013>
25. George C., Beeldens A., Barmpas F., Doussin J.F., Manganelli G., Herrmann H., Kleffmann J., Mellouki A. Impact of photocatalytic remediation of pollutants on urban air quality. *Frontiers of Environmental Science & Engineering*. 2016; 10(5): 2. <https://doi.org/10.1007/s11783-016-0834-1>
26. Gallus M., Akylas V., Barmpas F. et al. Photocatalytic de-pollution in the Leopold II tunnel in Brussels:  $NO_x$  abatement results. *Building and Environment*. 2015; 84: 125–133. <https://doi.org/10.1016/j.buildenv.2014.10.032>
27. Balykov A.S., Nizina T.A., Chugunov D.B., Davydova N.S., Kyashkin V.M. Photocatalysts based on Zn-Ti layered double hydroxide and its calcination products for self-cleaning concretes: Structure formation and photocatalytic activity. *Construction Materials and Products*. 2025; 8(1): 2. <https://doi.org/10.58224/2618-7183-2025-8-1-2>
28. Emeline A.V., Rudakova A.V., Sakai M., Murakami T., Fujishima A. Factors affecting UV-induced superhydrophilic conversion of  $TiO_2$  surface. *The Journal of Physical Chemistry C*. 2013; 117(23): 12086–12092. <https://doi.org/10.1021/jp400421v>
29. Tyukavkina V.V., Tsyryatyeva A.V. The structure of the cement stone modified by nanodispersed titanium-bearing additive. *Proceedings of the Fersman Scientific Session of the State Institute of the CSC RAS*. 2019; 16: 597–601. <https://doi.org/10.31241/FNS.2019.16.122>
30. Lukutsova N.P., Pykin A.A., Postnikova O.A., Golovin S.N., Borovik E.G. The structure of cement stone with dispersed titanium dioxide in daily age. *Bulletin of Belgorod State Technological University named after V.G. Shukhov*. 2016; 11: 13–17. <https://doi.org/10.12737/22432>
31. Strokova V., Ogurtsova Yu., Gubareva E., Nerovnaya S., Antonenko M. Multifunctional Anatase–Silica Photocatalytic Material for Cements and Concretes. *Journal of Composites Science*. 2024; 8(6): 207. <https://doi.org/10.3390/jcs8060207>
32. Li Y.-N., Chen Z.-Y., Bao S.-J., Wang M.-Q., Song C.-L., Pu S., Long D. Ultrafine  $TiO_2$  encapsulated in nitrogen-doped porous carbon framework for photocatalytic degradation of ammonia gas. *Chemical Engineering Journal*. 2018; 331: 383–388. <https://doi.org/10.1016/j.cej.2017.08.119>

33. Henderson M.A. A surface science perspective on TiO<sub>2</sub> photocatalysis. *Surface Science Reports*. 2011; 66: 185–297. <https://doi.org/10.1016/j.surfrep.2011.01.001>
34. Nakata K., Fujishima A. TiO<sub>2</sub> photocatalysis: Design and applications. *Journal of Photochemistry and Photobiology C: Photochemistry Reviews*. 2012; 13(3): 169–189. <https://doi.org/10.1016/j.jphotochemrev.2012.06.001>
35. Eddy D.R., Permana M.D., Sakti L.K., Sheha G.A.N., Solihudin, Hidayat S., Takei T., Kumada N., Rahayu I. Heterophase Polymorph of TiO<sub>2</sub> (Anatase, Rutile, Brookite, TiO<sub>2</sub> (B)) for Efficient Photocatalyst: Fabrication and Activity. *Nanomaterials*. 2023; 13(4): 704. <https://doi.org/10.3390/nano13040704>
36. Li Z., Cong S., Xu Y. Brookite vs Anatase TiO<sub>2</sub> in the Photocatalytic Activity for Organic Degradation in Water. *ACS Catalysis*. 2014; 4(9): 3273–3280. <https://doi.org/10.1021/cs500785z>
37. Monai M., Montini T., Fornasiero P. Brookite: Nothing New under the Sun?. *Catalysts*. 2017; 7(10): 304. <https://doi.org/10.3390/catal7100304>
38. Marchand R., Brohan L., Tournoux M. TiO<sub>2</sub> (B) a new form of titanium dioxide and the potassium octatitanate K<sub>2</sub>Ti<sub>8</sub>O<sub>17</sub>. *Materials Research Bulletin*. 1980; 15(8): 1129–1133. [https://doi.org/10.1016/0025-5408\(80\)90076-8](https://doi.org/10.1016/0025-5408(80)90076-8)
39. Zhao H., Liu L., Andino J.M., Li Y. Bicrystalline TiO<sub>2</sub> with controllable anatase–brookite phase content for enhanced CO<sub>2</sub> photoreduction to fuels. *Journal of Materials Chemistry A*. 2013; 1: 8209–8216. <https://doi.org/10.1039/C3TA11226H>
40. Kozhevnikova N.S., Ul'yanova E.S., Shalaeva E.V. et al. Low-Temperature Sol–Gel Synthesis and Photoactivity of Nanocrystalline TiO<sub>2</sub> with the Anatase/Brookite Structure and an Amorphous Component. *Kinetics and Catalysis*. 2019; 60(3): 325–336. <https://doi.org/10.1134/S002315841903008X>
41. Peng B., Zhu Z., Hu Z. et al. Removal of elemental mercury from simulated flue gas over MnO<sub>x</sub>/TiO<sub>2</sub> adsorbent: The synergistic effect of anatase and brookite TiO<sub>2</sub>. *Journal of Environmental Chemical Engineering*. 2025; 13(1): 115332. <https://doi.org/10.1016/j.jece.2025.115332>
42. Ohtani B., Prieto-Mahaney O.O., Li D., Abe R. What is Degussa (Evonik) P25? Crystalline composition analysis, reconstruction from isolated pure particles and photocatalytic activity test. *Journal of Photochemistry and Photobiology A: Chemistry*. 2010; 216: 179–182. <https://doi.org/10.1016/j.jphotochem.2010.07.024>
43. Zhu Q., Qian J., Pan H., Tu L., Zhou X. Synergistic manipulation of micro-nanostructures and composition: anatase/rutile mixed-phase TiO<sub>2</sub> hollow micro-nanospheres with hierarchical mesopores for photovoltaic and photocatalytic applications. *Nanotechnology*. 2011; 22(39): 395703. <https://doi.org/10.1088/0957-4484/22/39/395703>
44. Ohno T., Sarukawa K., Tokieda K., Matsumura M. Morphology of a TiO<sub>2</sub> Photocatalyst (Degussa, P-25) Consisting of Anatase and Rutile Crystalline Phases. *Journal of Catalysis*. 2001; 203(1): 82–86. <https://doi.org/10.1006/jcat.2001.3316>
45. Chalastara K., Demopoulos G.P. Selenate Se(VI) reduction to elemental selenium on heterojunctioned rutile/brookite nano-photocatalysts with enhanced charge utilization. *Chemical Engineering Journal*. 2022; 437(2): 135470. <https://doi.org/10.1016/j.cej.2022.135470>
46. Cao Y., Li X., Bian Z., Fuhr A., Zhang D., Zhu J. Highly photocatalytic activity of brookite/rutile TiO<sub>2</sub> nanocrystals with semi-embedded structure. *Applied Catalysis B: Environmental*. 2016; 180: 551–558. <https://doi.org/10.1016/j.apcatb.2015.07.003>
47. Jin H., You W., Tian K. et al. Construction of TiO<sub>2</sub>(B)/Anatase Heterophase Junctions via a Water-Induced Phase Transformation Strategy for Enhanced Photocatalytic Hydrogen Production. *Langmuir*. 2022; 38(49): 15282–15293. <https://doi.org/10.1021/acs.langmuir.2c02522>
48. Wang Z., Wang Y., Zhang W., Wang Z., Ma Y., Zhou X. Fabrication of TiO<sub>2</sub>(B)/Anatase Heterophase Junctions at High Temperature via Stabilizing the Surface of TiO<sub>2</sub>(B) for Enhanced Photocatalytic Activity. *The Journal of Physical Chemistry C*. 2019; 123(3): 1779–1789. <https://doi.org/10.1021/acs.jpcc.8b09763>
49. Zhu J., Zhu S., Kong X., Liang Y., Li Z., Wu S., Luo S., Chang C., Cui Z. Rutile-coated B-phase TiO<sub>2</sub> heterojunction nanobelts for photocatalytic H<sub>2</sub> evolution. *ACS Applied Nano Materials*. 2020; 3(10): 10349–10359. <https://doi.org/10.1021/acsnm.0c02263>
50. Eddy D.R., Sheha G.A.N., Permana M.D. Study on triphase of polymorphs TiO<sub>2</sub> (anatase/rutile/brookite) for boosting photocatalytic activity of metformin degradation. *Chemosphere*. 2024; 351: 141206. <https://doi.org/10.1016/j.chemosphere.2024.141206>
51. Kaplan R., Erjavec B., Dražić G., Grdadolnik J., Pintar A. Simple synthesis of anatase/rutile/brookite TiO<sub>2</sub> nanocomposite with superior mineralization potential for photocatalytic degradation of water pollutants. *Applied Catalysis B: Environmental*. 2016; 181: 465–474. <https://doi.org/10.1016/j.apcatb.2015.08.027>
52. Fischer K., Gaweł, A., Rosen D., Krause M., Abdul Latif A., Griebel J., Prager A., Schulze A. Low-Temperature Synthesis of Anatase/Rutile/Brookite TiO<sub>2</sub> Nanoparticles on a Polymer Membrane for Photocatalysis. *Catalysts*. 2017; 7(7): 209. <https://doi.org/10.3390/catal7070209>

53. An X., Hu C., Liu H., Qu J. Hierarchical nanotubular anatase/rutile/TiO<sub>2</sub> (B) heterophase junction with oxygen vacancies for enhanced photocatalytic H<sub>2</sub> production. *Langmuir*. 2018; 34(5): 1883–1889. <https://doi.org/10.1021/acs.langmuir.7b03745>

54. Ismagilov Z.R., Tsikoza L.T., Shikina N.V., Zarytova V.F., Zinoviev V.V., Zagrebelnyi S.N. Synthesis and stabilization of nano-sized titanium dioxide. *Russian Chemical Reviews*. 2009; 78(9): 873–885. <https://doi.org/10.1070/rc2009v078n09abeh004082>

55. Bulyga D.V., Evstropiev S.K. Kinetics of adsorption and photocatalytic decomposition of a diazo dye by nanocomposite ZnO–MgO. *Optics and Spectroscopy*. 2022; 130(9): 1176. <https://doi.org/10.21883/EOS.2022.09.54839.3617-22>

56. Fatimah I., Yahya A., Iqbal R.M., Tamyiz M., Doong R.-a., Sagadevan S., Oh W.-C. Enhanced Photocatalytic Activity of Zn-Al Layered Double Hydroxides for Methyl Violet and Peat Water Photooxidation. *Nanomaterials*. 2022; 12(10): 1650. <https://doi.org/10.3390/nano12101650>

57. Irani M., Mohammadi T., Mohebbi S. Photocatalytic Degradation of Methylene Blue with ZnO Nanoparticles; a Joint Experimental and Theoretical Study. *Journal of the Mexican Chemical Society*. 2016; 60(4): 218–225. <http://dx.doi.org/10.29356/jmcs.v60i4.115>

58. Khamizov R.Kh. A Pseudo-Second Order Kinetic Equation for Sorption Processes. *Russian Journal of Physical Chemistry A*. 2020; 94(1): 171–176. <https://doi.org/10.1134/S0036024420010148>

#### ADDITIONAL INFORMATION

The authors declare that generative artificial intelligence technologies and technologies based on artificial intelligence were not used in the preparation of the article.

#### INFORMATION ABOUT THE AUTHORS

**Artemy S. Balykov** – Cand. Sci. (Eng.), Associate Professor, Department of Building Constructions, National Research Mordovia State University, Saransk, Russia, [artbalrun@yandex.ru](mailto:artbalrun@yandex.ru), <https://orcid.org/0000-0001-9087-1608>

**Denis B. Chugunov** – Cand. Sci. (Chem.), Associate Professor, Department of Fundamental Chemistry and Chemical Technology, National Research Mordovia State University, Saransk, Russia, [iman081@gmail.com](mailto:iman081@gmail.com), <https://orcid.org/0000-0002-1612-0539>

**Vladimir M. Kyashkin** – Cand. Sci. (Phys.-Math.), Associate Professor, Senior Researcher, Department of Photonics, National Research Mordovia State University, Saransk, Russia, [kyashkin@mail.ru](mailto:kyashkin@mail.ru), <https://orcid.org/0000-0002-3413-247X>

**Natalia S. Davydova** – Laboratory Researcher, Research Laboratory of Ecological and Meteorological Monitoring, Building Technologies and Expertises, National Research Mordovia State University, Saransk, Russia, [davydowanatalia@yandex.ru](mailto:davydowanatalia@yandex.ru), <https://orcid.org/0009-0008-9409-682X>

#### CONTRIBUTION OF THE AUTHORS

**Artemy S. Balykov** – scientific leadership; development of the concept and development of study methodology; literature review; analysis of research results; writing the original text of the article; drawing up conclusions.

**Denis B. Chugunov** – development and optimization of technology for synthesis of titanium dioxide samples; collection and systematization of experimental data.

**Vladimir M. Kyashkin** – X-ray diffraction phase analysis of titanium dioxide samples; collection and systematization of experimental data.

**Natalia S. Davydova** – literature review; conducting experimental work; collection and systematization of experimental data.

#### The authors declare no conflicts of interests.

The article was submitted 28.03.2025; approved after reviewing 24.04.2025; accepted for publication 28.04.2025.